

Properties of a Single-Peripheral Model of the Deck Effect*

Ying-Yeung Yam

Department of Physics, College of William and Mary, Williamsburg, Virginia 23185

(Received 18 September 1972)

The properties of a single-peripheral model of the Deck effect are presented as a prototype diffraction-dissociation process, using $\pi N \rightarrow \pi \rho N$ as an example. The π - ρ mass spectrum, angular distributions, and the N - N momentum-transfer distribution are investigated. We evaluate the effects on these distributions due to three major components of the model, namely, the dissociation vertex, the propagation, and the diffraction scattering of the virtual particle. It is found that many "expected" properties (usually derived for asymptotic energies) of the diffraction-dissociation process do not obtain at finite energies. In particular, there is considerably more structure in the momentum-transfer and angular distributions. The mass dependence in the momentum-transfer slope found by others is reproduced in this model. Structure in the angular distributions is seen to imply some uncertainty over tests of helicity conservation for A_1 production. The peak in the mass spectrum (the Deck effect) is found to have an undesirable dependence on incident momentum. This difficulty is traced to the presence of spin in the model. Explicit numerical calculations and qualitative considerations lead us to believe that many Reggeized calculations of the Deck effect share the same difficulty. Their prediction of a sharp and s -independent peak is unjustified due to neglect of external spin.

I. INTRODUCTION

Diffraction processes¹ are of interest at high energies because the interaction is peripheral and the cross sections are large and approximately constant.² Furthermore, certain threshold enhancements such as the $N^*(1470)$, the $A_1(1080)$, and the $Q(1300)$ are presumably produced via diffractive processes although their status as genuine resonances have not been established.³ The basic difficulty is that such an enhancement may arise either (a) from a nonresonant production amplitude which peaks near threshold (i.e., some variation on the Deck effect⁴), (b) from a resonant production amplitude, or (c) from a coherent combination of peaking background and resonance production. In an earlier paper⁵ (RY), we presented a model for the nonresonant amplitude using, as an example, pion diffraction dissociation $\pi - \pi \rho$ as the dominant contribution to low π - ρ masses in the process

$$\pi + N \rightarrow \pi + \rho + N. \quad (i)$$

Our model cannot yet resolve the ambiguity about the origin of the enhancement. One reason is uncertainty over the parameters of the model. Another is a pathology in the model—an s -dependent mass spectrum—although, as we shall argue, this pathology can be present in other models. A more compelling reason is that the reaction, due to unitarity, between a resonance and its coherent background is known only for special cases in final-state interaction theory.⁶ In this paper, we study

the properties of the nonresonant amplitude through explicit numerical calculations, bearing in mind the fact that it is flexible enough to qualify either as a background to genuine resonance production or as the entire kinematic explanation of the enhancement.

Our model, represented by the three diagrams (A), (B), and (C) in Fig. 1, is essentially a single-peripheral process. It retains the elementarity of the virtual particle which scatters diffractively. In this respect, it differs with the double-peripheral model used by Berger and others,^{7,8} in which diagram 1(A) is not used but the virtual particles in 1(B) and 1(C) are Reggeized. Strictly speaking, the Berger-type model should be applicable only when all the final-state subenergies are high, and is preferred under such conditions since spin effects such as those due to the virtual vector meson in diagram 1(C) are better treated. However, it has been mostly applied to the low invariant π - ρ mass region as a "Reggeized Deck effect" and claimed to be able to account for the entire threshold (A_1) enhancement. Why Reggeon exchange will work at low subenergies is not clear. Presumably, some justification⁹ comes from the arguments of duality.¹⁰ But this justification is questionable on theoretical grounds,¹¹ and an experiment¹² involving charge exchange rather than diffraction scattering also casts some doubt on its validity. Conceptually, the conventional separation of background and resonance is of course lost if duality arguments are used. Any detailed structure besides that predicted by a Reggeon-exchange model

in the resonance region would be difficult to account for in such an approach. One may ignore duality and treat the Reggeon model as a conventional background amplitude to be added to the resonance production amplitude. But whether one can safely add the resonance amplitude to a *given* Reggeized background amplitude without overcounting is still a nagging but unsettled question. We mention for completeness that there exist more ambitious dual¹³ and nondual¹⁴ models which consider instead of reaction (i) the more general process

$$\pi + N \rightarrow 3\pi + N \quad (\text{ii})$$

in an attempt to satisfy crossing symmetry or Bose symmetry¹⁵ in the final 3π subsystem. We shall comment on these and Reggeized models further in Sec. IV.

In Sec. II, we review briefly the model and the parameters that are used to study its properties. In Sec. III, we present numerical results on the invariant π - ρ mass distribution, the squared-momentum-transfer $t_{p\alpha}$ distribution, and the angular distributions in the π - ρ rest frame for process (i) at 8 GeV/c incident pion momentum. We will study how the three major components in the model, namely, (a) the dissociation vertex, (b) the propagator, and (c) the diffraction scattering affect the distributions. The contribution from each diagram and the interference among them are noted. A report on the dependence on incident momentum leads to a discussion in Sec. IV on the relevancy of our model to three special topics of interest: (1) spin and Reggeon exchange, (2) mass dependence of the momentum-transfer slope, and (3) helicity conservation.¹⁶ The Appendix contains

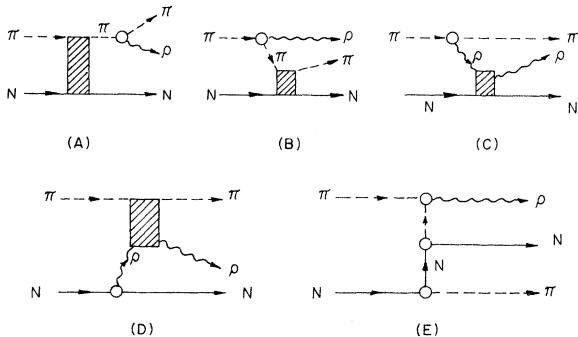


FIG. 1. Diagrams contributing to the background amplitude for $\pi N \rightarrow \pi\rho N$. (A), (B), and (C) are pion dissociation processes and are assumed dominant for low π - ρ masses. (D) is nucleon dissociation and (E) is non-diffractive exchange, and both are assumed negligible at low π - ρ masses. The shaded blob represents diffraction scattering

a brief description of the notation and kinematics used.

II. DETAILS OF THE MODEL

The notation and kinematics for process (i) are described in the Appendix where we also discuss how various kinematic quantities of interest are specified. In the rest frame of the final-state π - ρ system (see Fig. 2), the differential cross section is related to the invariant amplitude for process (i) by

$$\frac{d^4\sigma}{d\epsilon_{\beta\gamma} dt_{p\alpha} d\cos\theta_\gamma d\phi_\gamma} = \frac{1}{(4\pi)^4} \frac{|\vec{\gamma}|_{\vec{\beta}+\vec{\gamma}=0}}{|\vec{q}|_{\vec{p}=0}} |M_{fi}|^2. \quad (1)$$

The model used to calculate the nonresonant or background part B_{fi} of M_{fi} has been discussed in some detail in RY. We repeat the essential assumptions here for completeness.

(a) B_{fi} is given by the sum of the three diagrams (A), (B), and (C) in Fig. 1:

$$B_{fi} = M_A + M_B + M_C. \quad (2)$$

Processes such as nucleon dissociation $N \rightarrow N\rho$ and nondiffractive exchanges as illustrated by diagrams (D) and (E) in Fig. 1 are expected to be small in the kinematic region of interest and are therefore neglected.¹⁷ The background distributions are then obtained by substituting B_{fi} for M_{fi} in Eq. (1).

(b) The dissociation $\pi \rightarrow \pi\rho$ is common to all three diagrams. One of the particles at the dissociation vertex will be virtual. We treat it as an elementary particle with corresponding propagator and form factor. The following form factors are used for diagrams (A), (B) (see Ref. 18), and (C), respectively:

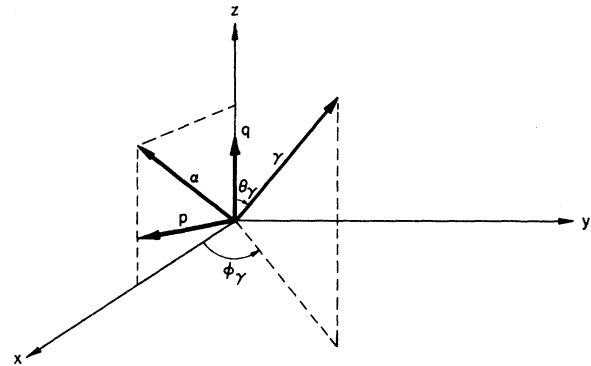


FIG. 2. Coordinate frame in the $\vec{\beta} + \vec{\gamma} = 0$ system for the process $q\bar{p} \rightarrow \alpha\beta\gamma$.

$$\begin{aligned}
F_A(s_{\beta\gamma}) &= \exp[\lambda_A(m_A^2 - s_{\beta\gamma})], \\
F_B(t_{q\beta}) &= [1 + \lambda_B |\vec{q}(m_\beta^2)|^2]^{1/2} / [1 + \lambda_B |\vec{q}(t_{q\beta})|^2]^{1/2}, \\
F_C(t_{q\gamma}) &= \exp[\lambda_C(t_{q\gamma} - m_C^2)],
\end{aligned} \tag{3}$$

where

$$\begin{aligned}
|\vec{q}(t_{q\beta})|^2 &= [t_{q\beta} - (m_q - m_\beta)^2] \\
&\quad \times [t_{q\beta} - (m_q + m_\beta)^2] / 4m_\beta^2.
\end{aligned}$$

There are, of course, other possible choices¹⁹ such as those used by Jackson and Pilkuhn²⁰ and that given by Benecke and Dürr.²¹ We have not tested all of them in our calculation.²² Obviously, more reliable form factors must be found if a comparison to experiment is to be detailed and convincing. Our choice is intended to illustrate the possible effects only.

(c) The elastic scattering off the target nucleon is assumed to be diffractive and imaginary. For simplicity, the nucleons are taken to be spinless while the ρ -spin dependence in ρ - N scattering is taken as δ_{uv} . Explicitly, the elastic scattering amplitude is of the form:

$$f = i [|\vec{k}|_{\text{c.m.}} \theta(|\vec{k}|_{\text{c.m.}} - k^c) \sigma_T / 4\pi] e^{at_p \alpha/2}, \tag{4}$$

where $|\vec{k}|_{\text{c.m.}}$ is the momentum in the appropriate center-of-mass frame, σ_T is the total cross section, and a is the diffraction slope of the corresponding elastic scattering. We have inserted a step function, $\theta(|\vec{k}|_{\text{c.m.}} - k^c)$ with a cutoff k^c . This is a crude way to insure that only diffractive scattering off the nucleon is used. Because the diffraction scattering is off the mass shell, there is actually some ambiguity in choosing the center of mass momentum $|\vec{k}|_{\text{c.m.}}$ in Eq. (4). We remove this ambiguity by using only the momentum of the recoil nucleon in the appropriate center-of-mass frame; viz. for diagram A, we take $|\vec{k}|_{\text{c.m.}} = |\vec{\alpha}_A|$, where $|\vec{\alpha}_A|$ is defined in Eq. (6) below. For fixed s , this choice will suppress the contribution to high π - ρ masses as the virtual particle goes far off the mass shell.

(d) The parameters of the model are then $\sigma_T^{\pi N}$, $\sigma_T^{\rho N}$, $a_{\pi N}$, $a_{\rho N}$, λ_A , λ_B , λ_C , α_A^c , α_B^c , α_C^c , and $g_{\rho\pi\pi}$, the $\rho\pi\pi$ coupling constant. Experimentally, most of the parameters are known²³: $g_{\rho\pi\pi}^2/4\pi \approx 2.4$, and for the GeV region, $\sigma_T^{\pi N} \approx \sigma_T^{\rho N} \approx 30$ mb, $a_{\pi N} \approx a_{\rho N} \approx 7$ (GeV/c)⁻², and $\alpha_i^c \approx 0.7$ GeV/c. These approximate numbers will suffice since we are not attempting a fit to data. Note however that the λ_i 's remain arbitrary.

The amplitudes for diagrams (A), (B), and (C) of Fig. 1 can now be written down explicitly as

$$\begin{aligned}
M_A &= (2\epsilon^\lambda \cdot \gamma) \frac{g_{\rho\pi\pi} F_A(s_{\beta\gamma})}{s_{\beta\gamma} - m_A^2} \\
&\quad \times \left[\frac{w |\vec{\alpha}_A|}{m_p} \theta(|\vec{\alpha}_A| - \alpha_A^c) \sigma_T^{\pi N} e^{a_{\pi N} t_p \alpha/2} \right], \\
M_B &= (2\epsilon^\lambda \cdot q) \frac{g_{\rho\pi\pi} F_B(t_{q\beta})}{t_{q\beta} - m_B^2} \\
&\quad \times \left[\frac{(s_{\gamma\alpha})^{1/2} |\vec{\alpha}_B|}{m_p} \theta(|\vec{\alpha}_B| - \alpha_B^c) \sigma_T^{\pi N} e^{a_{\pi N} t_p \alpha/2} \right], \\
M_C &= (u\epsilon^\lambda \cdot q + v\epsilon^\lambda \cdot \gamma) \frac{g_{\rho\pi\pi} F_C(t_{q\gamma})}{t_{q\gamma} - m_C^2} \\
&\quad \times \left[\frac{(s_{\alpha\beta})^{1/2} |\vec{\alpha}_C|}{m_p} \theta(|\vec{\alpha}_C| - \alpha_C^c) \sigma_T^{\rho N} e^{a_{\rho N} t_p \alpha/2} \right],
\end{aligned} \tag{5}$$

where:

$$\begin{aligned}
u &= 1 - (m_q^2 - m_\gamma^2) / m_C^2, \\
v &= 1 + (m_q^2 + m_\gamma^2) / m_C^2, \\
|\vec{\alpha}_A|^2 &= [s_{\beta\gamma} - (w - m_\alpha)^2] [s_{\beta\gamma} - (w + m_\alpha)^2] / 4s, \\
|\vec{\alpha}_B|^2 &= [s_{\alpha\gamma} - (m_\alpha - m_\gamma)^2] [s_{\alpha\gamma} - (m_\alpha + m_\gamma)^2] / 4s_{\alpha\gamma}, \\
|\vec{\alpha}_C|^2 &= [s_{\beta\alpha} - (m_\beta - m_\alpha)^2] [s_{\beta\alpha} - (m_\beta + m_\alpha)^2] / 4s_{\beta\alpha}.
\end{aligned} \tag{6}$$

An approximate version of this background amplitude in which only diagrams (B) and (C) of Fig. 1 are used has been given by Stodolsky.²⁴ The approximation is based on a kinematic relation [see Eqs. (2) and (3) of Ref. 24]:

$$\begin{aligned}
\frac{|\vec{q}|_{\vec{p}=0}}{s_{\beta\gamma} - m_q^2} &\approx - \frac{|\vec{\gamma}|_{\vec{p}=0}}{t_{q\beta} - m_B^2} \\
&\approx - \frac{|\vec{\beta}|_{\vec{p}=0}}{t_{q\gamma} - m_C^2}
\end{aligned} \tag{7}$$

which is valid for high-energy, small-angle scattering of the virtual mesons in diagrams (B) and (C) of Fig. 1. There are still simpler models for the background amplitude. We list four here for later comparison.

- (i) $B_{fi} \approx \text{constant}$,
- (ii) $B_{fi} \approx \text{constant} \times \exp(\frac{1}{2} \bar{a} t_p \alpha)$,
- (iii) $B_{fi} \approx \text{constant} / (s_{\beta\gamma} - m_q^2)$,
- (iv) $B_{fi} \approx \text{constant} \times \exp(\frac{1}{2} \bar{a} t_p \alpha) / (s_{\beta\gamma} - m_q^2)$,

where $\bar{a} \approx 7$ (GeV/c)⁻². Among these, model (i) yields the kinematic phase space, while models (ii), (iii), and (iv) represent different "explanations" for the origin of the Deck effect. The oldest explanation,²⁵ that the sharply peaked diffraction scattering is responsible for the enhancement at low subenergies, is represented by (ii). Stodolsky's argument that a $1/(s_{\beta\gamma} - m_q^2)$ factor is the dominant mechanism is represented by (iii). (iv) is a combination of (ii) and (iii) and is the approximate amplitude of Stodolsky with further neglect of structure, spin, and interference effects.

III. RESULTS

A. Mass Spectrum

A typical π - ρ mass spectrum in our model at 8 GeV/c incident momentum is shown in Fig. 3. The following general features of the model described in RY are evident: (a) each diagram contributes a "Deck effect," (b) all three diagrams are comparable in magnitude, and (c) a destructive interference between Fig. 1(A) and the other two diagrams results in the total background [Eq. (2)] peaking closer to threshold than the individual diagrams. Qualitatively, this cancellation can be seen in the kinematic relation Eq. (7), and represents a unitary correction in the 0^- (p -wave) state provided by diagram 1(A). Were we to attempt a comparison to data on the A_1 enhancement, we would find the peak too far out (≈ 1.35 GeV) and too wide (≈ 1 GeV). Therefore, it is of interest to see how sensitive our model is to changes in its parameters.

Reasonable changes in the diffraction scattering parameters (σ_T , a , and α^e) produce predictable but insignificant changes. For example, increasing $\sigma_T^{\rho N}$ from 30 mb to 60 mb moves the peak out

to 1.5 GeV. Changing $a_{\pi N} = a_{\rho N}$ from 7 (GeV/c) $^{-2}$ to 10 (GeV/c) $^{-2}$ moves the peak inward to 1.28 GeV. In short, the peak position and width have at best 10% variations (with larger variations in magnitude, of course) for 40–100% variations in σ_T and a . The cutoff α_i^e suppress high π - ρ masses. But at 8 GeV incident energy, the effect is less than 10% on peak position, width, or magnitude and gets smaller with increasing energy. A similar comment applies to our choice of $|\vec{k}|_{c.m.}$ in Eq. (4) to remove an off-mass-shell ambiguity.

A form factor enhances the probability for the virtual particle to have diffraction kinematics and is thus expected to sharpen the peak. Our calculation substantiates this observation. For example, from no form factors ($\lambda_A = \lambda_B = \lambda_C = 0$) to fairly strong form factors [$\lambda_A = \lambda_C = 1.0$ (GeV/c) $^{-2}$, $\lambda_B = 49.0$ (GeV/c) $^{-2}$], we can change the magnitude by an expected factor of 2 or 3 and the position and width by as much as 30%. Were we now to fit this to the A_1 , we would find our prediction lower and flatter in the A_1 region. More seriously, a form factor, unless it has mass dependence¹⁹ built in, loses its effectiveness as the incident energy increases. Most of our later observations are based

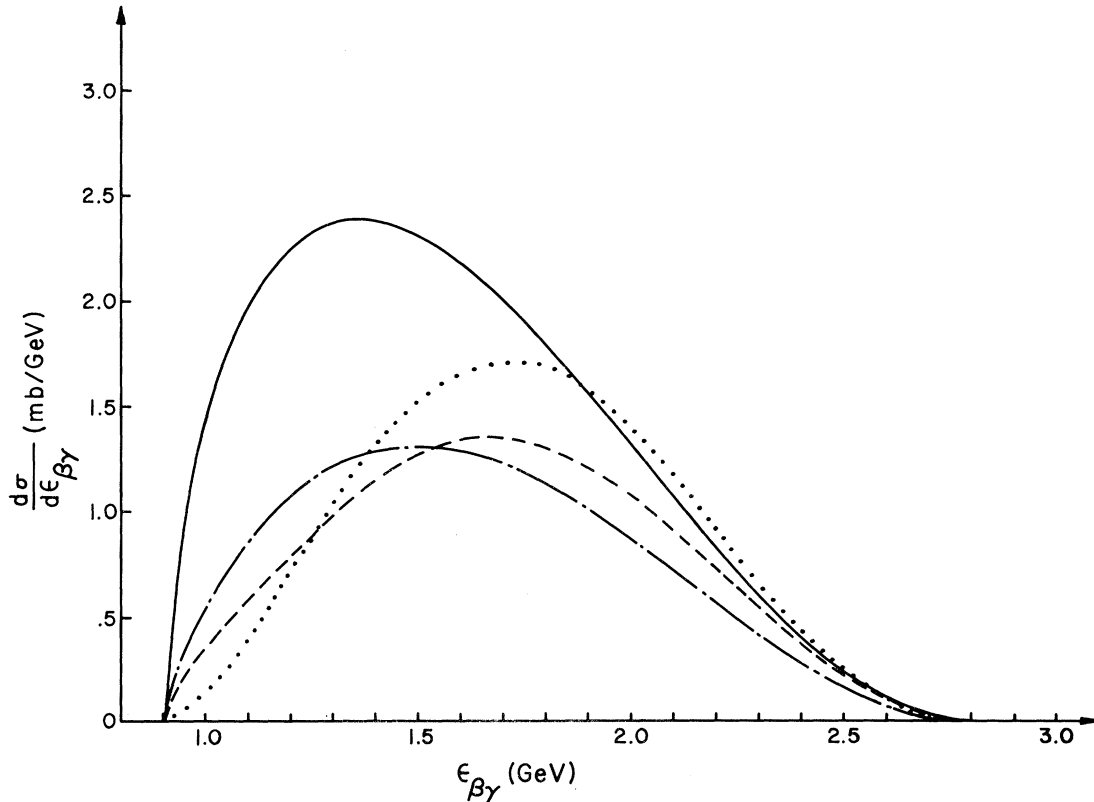


FIG. 3. Contributions from diagrams (A) (···), (B) (---), (C) (---) to the background (—) at 8 GeV/c incident momentum are given separately. Parameters used are: $\sigma_T^{\pi N} = \sigma_T^{\rho N} = 30$ mb, and $a_{\pi N} = a_{\rho N} = 7$ (GeV/c) $^{-2}$. No form factors ($\lambda_A = \lambda_B = \lambda_C = 0$) or cutoffs ($\alpha_A^e = \alpha_B^e = \alpha_C^e = 0$) are used.

on calculations without arbitrary form factors.

According to Stodolsky,²⁴ each propagator contributes, via Eq. (7), a $1/(s_{\beta\gamma} - m_a^2)$ factor which is the dominant mechanism for threshold peaking. Models (iii) and (iv) of Eq. (8) contain the essence of this mechanism. We present in Fig. 4 the numerical results for models (i)–(iv) and our model, Eqs. (2), (5). It can be seen that both diffraction scattering [model (ii)] and the propagator factor [model (iii)] produce distortions of phase space, but the propagator leads to a peak closer to threshold and sharper, in support of the Stodolsky mechanism. Somewhat of a surprise is the fact that our model, though more complicated, actually has a peak farther out and flatter. Now, since the simpler models are essentially spinless versions of our model, one immediately surmises that the ρ spin in our model is shifting and widening the peak. We shall show in Sec. IV why spin can render the Stodolsky mechanism inoperative.

B. Momentum-Transfer Distribution

We expect that the distribution for the square of the momentum transfer to the target nucleon $t_{p\alpha}$

to be characterized by the input diffraction scattering off the nucleon. In fact, the approximation of Eq. (7), when applied to our model, implies that the same $t_{p\alpha}$ dependence obtains for each diagram. But the numerical calculation indicates that there are sharp deviations.

For a given π - ρ mass $\epsilon_{\beta\gamma}$ and small values of $t_{p\alpha}$, the calculated distribution can be represented as

$$\frac{d^2\sigma}{d\epsilon_{\beta\gamma} dt_{p\alpha}} \simeq A \exp(bt_{p\alpha}) \quad (9)$$

for

$$t_{p\alpha}^{(+)} - 0.3 \text{ (GeV}/c)^2 \leq t_{p\alpha} \leq t_{p\alpha}^{(+)} ,$$

where A and b are different for different diagrams. In Fig. 5(a), we plot the resultant slope b as a function of the π - ρ mass for each diagram. A sharp deviation, which depends on π - ρ mass, from the input value $a_{\pi N} = a_{\rho N} = 7 \text{ (GeV}/c)^{-2}$ is present at low π - ρ masses for diagram 1(B). An explanation of this deviation has been given for a similar process by Oh and Walker.²⁶ There are also large deviations for diagram 1(C) due in part to spin effects associated with the virtual ρ . Form factors

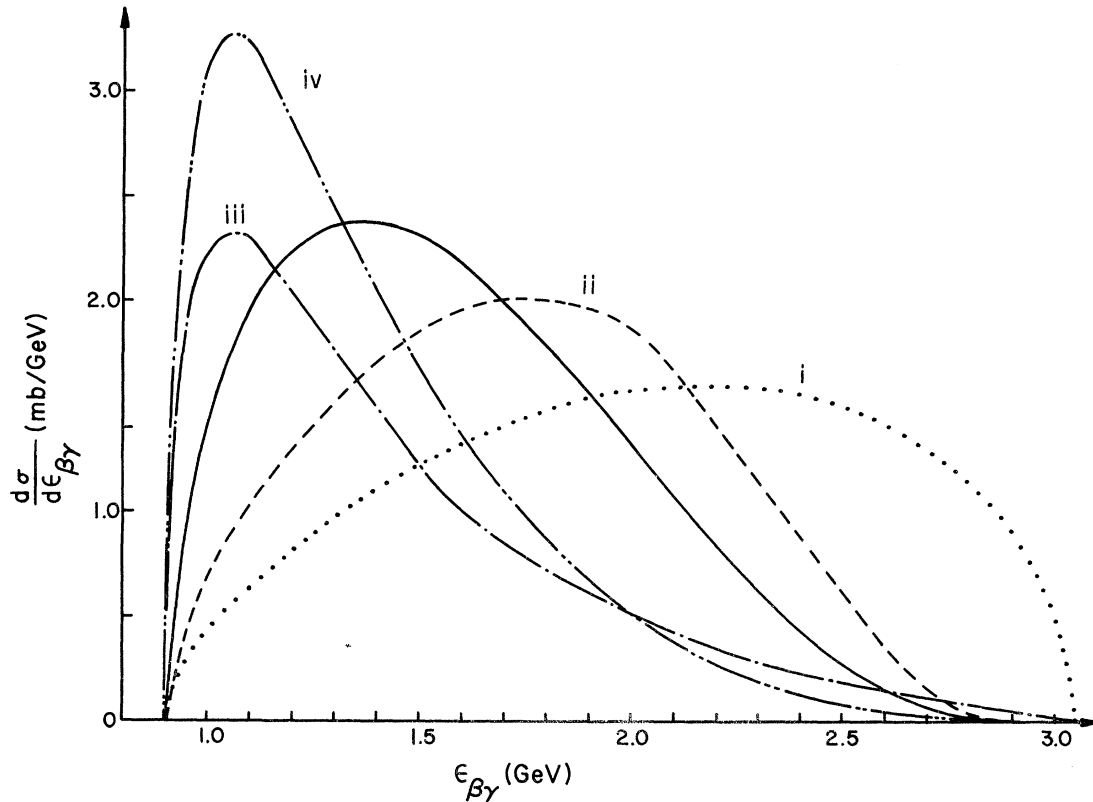


FIG. 4. Comparison of our model (—) with the simpler models of Eq. (8): (i) (···), (ii) (---), (iii) (-·-), and (iv) (-··-), at 8 GeV/c incident momentum. Parameters used for our model are: $\sigma_T^{\pi N} = \sigma_T^{\rho N} = 30 \text{ mb}$, $a_{\pi N} = a_{\rho N} = 7 \text{ (GeV}/c)^{-2}$, $\lambda_A = \lambda_B = \lambda_C = 0$, and $\alpha_A^c = \alpha_B^c = \alpha_C^c = 0$. Cross sections for models (i)–(iv) are in arbitrary units.

enhance the deviation [see Fig. 5(b)], and the deviations persist at higher energies [see Fig. 5(c)]. We shall discuss the slope b further in Sec. IV.

In changing the parameters of the model, the effects on $d\sigma/dt_{p\alpha}$ are similar to those on $d\sigma/d\epsilon_{\beta\gamma}$. That is, the magnitude changes in the expected way, but the shape, as characterized by a slope for example, changes only by about 10%. Off-mass-shell corrections are more effective in suppressing higher momentum transfer values. Consequently, the characteristic slope can change by 15% to 20%. Of some interest also is the momentum-transfer distribution $d\sigma/dt_{p\alpha}$ integrated over a range of π - ρ masses. We find a turn-over at low $t_{p\alpha}$ due to an $\epsilon_{\beta\gamma}$ dependence in $t_{p\alpha}^{(\pm)}$ [see Eq. (A2)]. The distribution becomes flatter as higher π - ρ mass states are included, as is to be expected from Fig. 5.

C. Angular Distribution

The approximation in Eq. (7), when applied to our model, suggests that there is isotropy in the azimuthal distribution for the π - ρ system in its own rest frame. This isotropy has been noted in RY to be a general property of diffraction-dissociation processes where the incident particle, such as a π , carries no azimuthal information. Furthermore, the π - ρ system is dominantly $J^P = 1^+$ (s wave). Consequently, it is argued in RY that the polar distribution is also approximately isotropic, leading to a $\cos^2\theta$ decay distribution for the ρ . In the numerical calculations, these expected isotropies are not born out. Figure 6 demonstrates that there are structures in the angular distributions. The kinematic factor $|\vec{k}_{c,m}|$ from diffraction scattering is responsible for the azimuthal anisotropy in our model. The difference in the contributions from diagrams 1(B) and 1(C) to $d\sigma/d\phi_\gamma$ reflects the difference in the ϕ_γ dependence of $|\vec{\alpha}_B|$ and $|\vec{\alpha}_C|$. The polar distribution generally favors forward ($\theta_\gamma \approx 0$) angles. That this is true even for diagram 1(B), where a backward ($\theta_\gamma \approx \pi$) peak is expected from the propagator, suggests that the forward peak is governed by other factors—spin effects and the $|\vec{k}|$ factor from diffraction scattering. A smaller backward peak appears at high π - ρ masses. Angular distributions integrated over a range of π - ρ masses in the A_1 region exhibit similar behavior.

Changes in the input total cross section or diffraction slope will alter the over-all magnitude, of course. But they can alter the shape mostly through interference effects. From our experience with the mass spectrum, we expect such changes to be small. On the other hand, changes in the cutoff momentum α_B^c, α_C^c will affect allowed

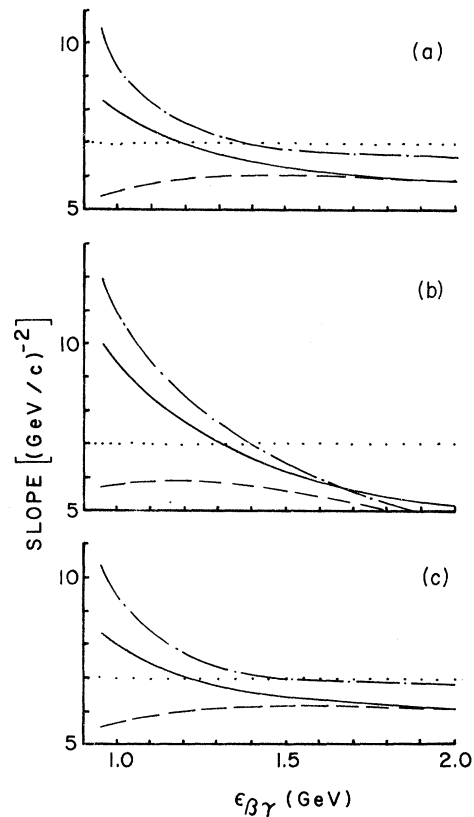


FIG. 5. Dependence of the diffraction slope on π - ρ mass with (a) no form factors at 8 GeV/c; (b) form factor effects at 8 GeV/c; and (c) no form factors at 20 GeV/c incident momentum. Contributions from diagrams (A) (\cdots), (B) ($-\cdot-$), and (C) ($---$) to the background ($---$) are given separately. Parameters used are: $\sigma_{\pi N}^{\pi} = \sigma_{\rho N}^{\rho} = 30$ mb, $\alpha_{\pi N} = \alpha_{\rho N} = 7$ (GeV/c) $^{-2}$, and $\alpha_A^c = \alpha_B^c = \alpha_C^c = 0$. For (a) $\lambda_A = \lambda_B = \lambda_C = 0$; (b) $\lambda_A = \lambda_C = 1.0$ (GeV/c) $^{-2}$, $\lambda_B = 49.0$ (GeV/c) $^{-2}$; (c) $\lambda_A = \lambda_B = \lambda_C = 0$.

values of $|\vec{k}_B|$ and $|\vec{k}_C|$ and thus the shape of both angular distributions directly. Similarly, form factors, which introduce additional $\cos\theta_\gamma$ dependence into the final π - ρ state, will alter the shape of the polar distributions. Numerical calculations indicate that the effect is indeed considerable, with less peaking in the forward $\theta_\gamma \approx 0$ angles, especially for diagram 1(B), as one would expect from the θ_γ dependence of the variable t_{qB} .

D. Dependence on Incident Energy

Our calculation in Secs. IIIA–IIIC has been made at an incident pion momentum of 8 GeV/c. As the incident momentum gets higher, we expect the kinematic relation Eq. (7) to be a better approximation for a fixed value of the π - ρ invariant mass. Consequently, the azimuthal distribution should approach isotropy. And, in the absence of form

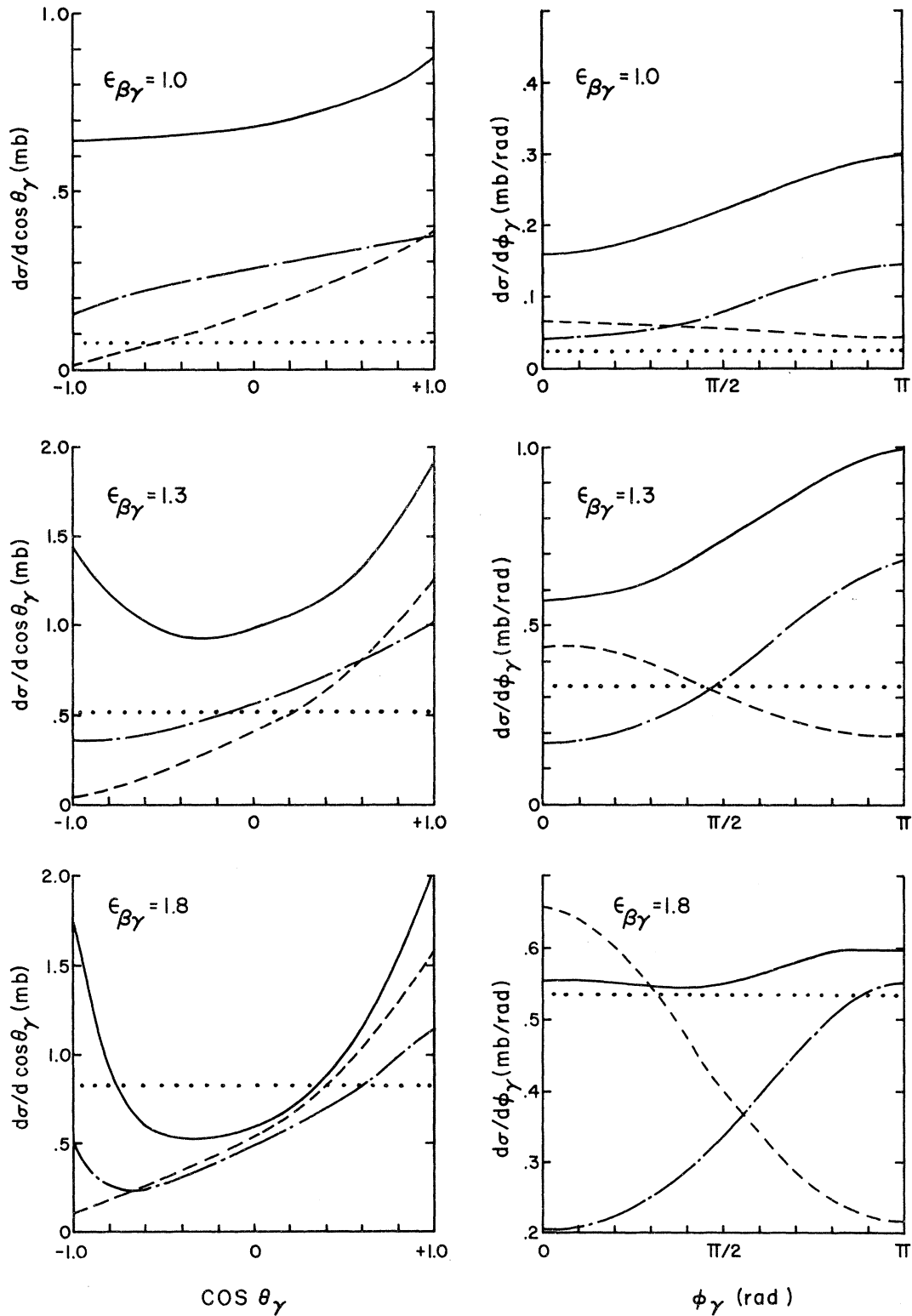


FIG. 6. Angular distributions at $\epsilon_{\beta\gamma} = 1.0, 1.3,$ and 1.8 GeV, respectively, for 8 GeV/ c incident momentum. Contributions from diagrams (A) (\cdots), (B) ($---$), and (C) ($- \cdot -$) to the background ($---$) are given separately. Parameters used are: $\sigma_T^{\pi N} = \sigma_T^{\rho N} = 30$ mb, $a_{\pi N} = a_{\rho N} = 7$ (GeV/ c) $^{-2}$, $\lambda_A = \lambda_B = \lambda_C = 0$, and $\alpha_A^c = \alpha_B^c = \alpha_C^c = 0$.

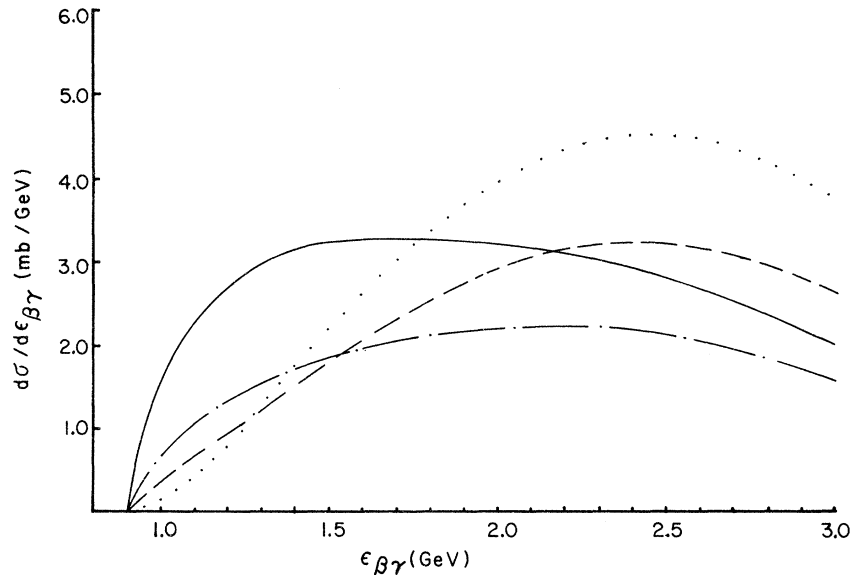


FIG. 7. Mass spectrum at 20 GeV/c incident momentum. Contributions from diagrams (A) (\cdots), (B) ($-\cdots$), and (C) ($-\cdots$) to the background ($—$) are given separately. Parameters used are: $\sigma_{\pi N}^{\pi N} = \sigma_{\rho N}^{\rho N} = 30$ mb, $a_{\pi N} = a_{\rho N} = 7$ (GeV/c) $^{-2}$, $\lambda_A = \lambda_B = \lambda_C = 0$, and $\alpha_A^c = \alpha_B^c = \alpha_C^c = 0$.

factor and spin effects, it is expected that the polar distribution should do likewise. However, numerical calculation using the same parameters shows that structures in the angular distributions persist at the momentum (20 GeV/c) considered. Furthermore, the mass dependence of the momentum transfer slope also persists [see Fig. 5(c)]. But the most serious difficulty in the model is associated with the shape of the mass spectrum as the incident energy increases. We see from Fig. 7 that the peak moves away from the threshold and becomes wider as the incident energy increases. The resultant total production cross section for process (i) thus grows unreasonably with rising incident energy. This difficulty is not alleviated by the use of the form factors in Eq. (3) even though their effect on angular distributions is considerable. We have not investigated in detail whether more drastic choices of form factors¹⁹ would remedy the situation. The difficulty can be traced to the presence of spin, the ρ spin in our case. In Fig. 8, we present a spinless calculation where internal and external spins are ignored. It can be seen that, indeed, the peak does *not* move with rising incident energy. The shape and the total production cross section remains quite stable over a range of 10^4 GeV in incident energy. Thus, the difficulty in obtaining an s -independent peak is closely related to the presence of spin in the model. In Sec. IV, we shall comment on it and the relevancy of Reggeized models with regard to the presence of spin. We mention, for later reference, the fact that Eq. (8) for models (iii) and (iv) clearly

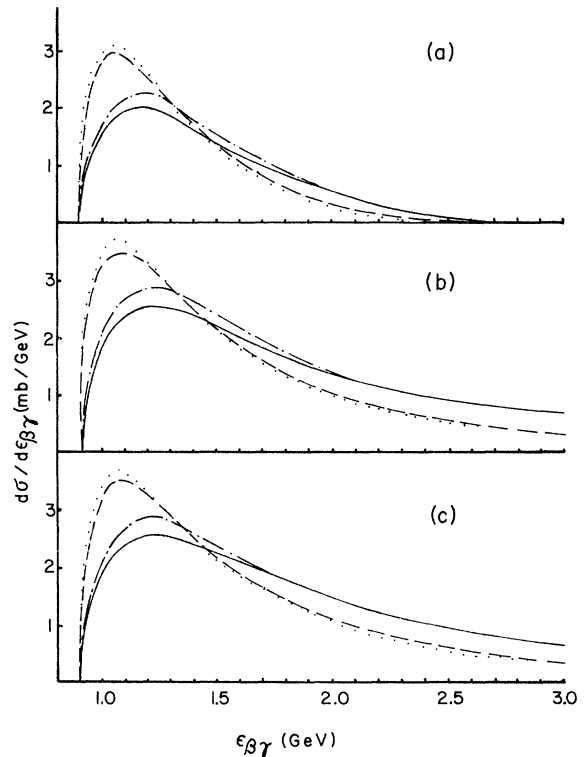


FIG. 8. Spinless calculation with incident momentum at (a) 8 GeV/c, (b) 64 GeV/c, and (c) 10^4 GeV/c. Contributions from diagrams (A) (\cdots), (B) ($-\cdots$), and (C) ($-\cdots$) to the background ($—$) are given separately. Parameters used are: $\sigma_{\pi N}^{\pi N} = \sigma_{\rho N}^{\rho N} = 30$ mb, $a_{\pi N} = a_{\rho N} = 7$ (GeV/c) $^{-2}$, $\lambda_A = \lambda_B = \lambda_C = 0$, and $\alpha_A^c = \alpha_B^c = \alpha_C^c = 0$.

indicates no s dependence for peaks generated by the Stodolsky mechanism.

IV. DISCUSSION

As suggested by the diagrams 1(B) and 1(C), there is a very simple picture of a dissociation process, say, $\pi \rightarrow \pi\rho$. In this picture, the initial π state dissociates into its component states π , $\pi\rho$, etc., which are scattered back on the mass shell to form various final states, among them, the final physical $\pi\rho$ states. The scattering back on the mass shell is most probable if it is via diffraction scattering off a target—a process where the target plays a minimal and most inert role. One of the basic notions behind this picture is the “expectation” that the final *physical* $\pi\rho$ state is not much different from the initial *virtual* $\pi\rho$ state which is part of the initial physical π state. In fact, the closer the final $\pi\rho$ mass is to the initial π mass, the closer is the “expected” resemblance. Such “expectations” form the intuitive basis within which the diffraction dissociation process is often visualized and understood. In our model, many “expected” properties can be derived explicitly by applying Eq. (7). But our numerical calculation has revealed many deviations. We discuss here some deviations of interest.

A. $\epsilon_{\beta\gamma}$ Dependence of $t_{p\alpha}$ Distribution

For example, one would “expect” the momentum-transfer distribution for the scattering of the initial π state into a low-mass final $\pi\rho$ state to closely resemble that for the input diffraction scattering of the virtual (π and ρ) components in the initial π state. If the momentum-transfer distribution is as parametrized in Eq. (9), then we “expect” the slope b for each diagram to be the same as the input diffraction slope a in Eq. (4) and to be independent of the $\pi\rho$ invariant mass. But in fact, Fig. 5 shows that this “expectation” is not realized. The deviation is sharpest at lower $\pi\rho$ masses. Such a mass dependence in the slope has been observed experimentally in the production of nucleon resonances²⁷ and in threshold enhancements²⁸ like the A_1 , Q , and $N^*(1470)$. Elitzür,²⁹ using scaling and a model of nucleon structure, derives an explicit formula relating the slope to the nucleon resonance mass. The predicted slopes are generally smaller³⁰ than the input nucleon-diffraction scattering slope. An explanation of the mass dependence of the slope for dissociation processes has been given by Oh and Walker²⁶ within the context of an elementary particle model such as ours. The propagator in diagram 1(B) introduces through kinematics a sharper $t_{p\alpha}$ dependence, predicting slopes which at low $\epsilon_{\beta\gamma}$ values

are generally larger³¹ than the input diffraction slope (see Fig. 5). Essentially the same reason has been given by Berger³² for the Reggeized version. The same general mass dependence is also observed in dual model calculations.³³ But, no simple explicit formula, like that of Elitzür, has been proposed. Indeed, short of an explicit calculation in each case, we do not have a grasp of how the mass dependence of b changes as we change the parameters in the dissociation process. For example, one may ask whether the same mass dependence obtains for the dissociation $\pi \rightarrow \pi\rho$ if nucleon targets are replaced by nuclear targets.³⁴ Or, whether the mass dependence is sensitive to the detailed nature of very similar dissociated subsystems, say, between $K \rightarrow K^*\pi$ and $K \rightarrow K\rho$. Or whether the mass dependence changes as the incident energy changes. On this last question, at least, something qualitative can be said. For sufficiently high s , the relation in Eq. (7) should hold and the propagator will cease to contribute to a sharper $t_{p\alpha}$ dependence. The $t_{p\alpha}$ distribution should then be identical to the input diffraction scattering distribution for each diagram.³¹ In this limit, there is no dependence on the final $\pi\rho$ mass (as long as it is low) or on the character of all particles (as long as the input diffraction scattering is the same). Unfortunately, this observation is hard to check. Eq. (7) may be a truly asymptotic limit, not realizable at finite energies. Form factor and spin effects introduce competing $t_{p\alpha}$ dependences, and energy dependence in the input slope further confuses the picture. Our spinless model shows that at 10^4 GeV/ c incident momentum, the mass dependence has not completely disappeared.

B. Anisotropic Angular Distributions

Flat distribution in the azimuthal angle ϕ has often been expected as a property of π - or K -initiated diffraction dissociation processes. Within our model, it can be obtained by applying the approximation in Eq. (7) together with high sub-energies. In particular, since our coordinate frame corresponds to the so-called “Gottfried-Jackson” frame,³⁵ a nonuniform distribution in ϕ would be considered as evidence against the “conservation¹⁶ of t -channel helicities.” In fact, such a criterion has been used in testing³⁶ the helicity conservation hypothesis for diffractively produced “resonances” such as the A_1 and Q . However, our detailed calculation shows (see Fig. 6), that flat distributions in ϕ at finite incident energies are in general not obtained for diagrams 1(B) and 1(C). The reason for the nonflatness in our model is simply due to the factors $|\tilde{\alpha}_B|$ and $|\tilde{\alpha}_C|$ in Eq. (6)

which are dependent on ϕ through the subenergy variables $s_{\beta\alpha}$ and $s_{\gamma\alpha}$. Regge models have the same factors. A nonflat ϕ distribution considerably clouds the picture regarding t -channel helicity conservation for the case of the A_1 or Q where no separation of "resonance" and background is performed on the experimental data. If the A_1 is considered a resonance to be separated from a background, then a model such as ours serves as the dominant background. If the A_1 is considered the dual to a cross-channel Reggeon, then of course, there is no background. But in either case, there is, theoretically, ϕ anisotropy, which will be hard to separate out in a model-independent way. Similar results are obtained if we examine the amplitudes in the over-all center-of-mass frame as directed by considerations of s -channel helicity conservation.¹⁶ Here, it is the propagator and form factor in diagrams 1(B) or 1(C) which lead to a corresponding ϕ anisotropy. In any case, we believe that ϕ tests of helicity conservation in multiparticle final states are not reliable unless certain kinematic conditions, such as those needed for Eq. (7) to hold, are satisfied.³⁷

The polar distribution also furnishes certain information regarding helicity conservation that is usually extracted in the form of density matrix elements, $\rho_{mm'}$. For the production $\pi \rightarrow A_1$, t -channel helicity conservation implies¹⁶ that only ρ_{00} is expected to be nonzero in the Gottfried-Jackson frame. An isotropic polar distribution in the subsequent s -wave dissociation $A_1 \rightarrow \pi\rho$ is expected to result. Our calculation (see Fig. 6) again indicates that these expectations are not realized. There is structure in the A_1 region which can be understood qualitatively in our model on the basis of opposing effects from the propagator and form factor on the one hand, and spin and a diffraction scattering factor [$|k|$ in Eq. (4)] on the other. Anisotropy is also obtained in a Reggeon model,³² although the shape is, as expected, different because of a different momentum-transfer dependence. Clearly, the same difficulty and ambiguity³⁸ surrounding ϕ tests are present in θ tests of helicity conservation for resonances not separated from the multiparticle final state background.

C. Spin and the Mass Spectrum

In the Stodolsky mechanism,²⁴ it is the closeness of the final π - ρ state to the initial π state which is expected to cause threshold peaking in the π - ρ mass spectrum. Our results in Figs. 4 and 7 however, demonstrate that the single-peripheral model with a ρ spin fails to exhibit the expected dominance by a Stodolsky mechanism, while a spinless

version does exhibit it. We propose a more general but nevertheless kinematic mechanism. In what follows, we will attempt to show through qualitative but model-independent arguments that whatever controls the high π - ρ mass behavior will determine the essential features of the Deck effect. This controlling factor will be strongly spin-dependent and will be different for different (spinless, single peripheral, and Reggeized) models.

For ease of reference we write the β - γ mass spectrum for each diagram of topology (A) or (B) in Fig. 1 as

$$\frac{d\sigma}{d\epsilon_{\beta\gamma}} = |\vec{\gamma}|^N \times \mathcal{P} \times \mathcal{F} \times \mathcal{R}, \quad (10)$$

where N , \mathcal{P} , \mathcal{F} , \mathcal{R} are factors affecting the mass spectrum which are, in general, diagram- and model-dependent. N represents threshold effects due to phase space ($N=1$) and spin ($N \geq 1$); \mathcal{P} represents the effect of the virtual particle propagator, Reggeized and otherwise; \mathcal{R} represents additional spin and phase space effects which cause the mass spectrum to rise at high $\epsilon_{\beta\gamma}$ values and \mathcal{F} represents effects such as diffraction scattering, form factor, cutoff, phase-space limit, or any other correction which cause the mass spectrum to fall off at high $\epsilon_{\beta\gamma}$. An integration over angular and momenta-transfer dependences is assumed. If we assume the factors \mathcal{P} , \mathcal{F} , and \mathcal{R} to be smooth functions of $\epsilon_{\beta\gamma}$, then within the kinematic limits of $\epsilon_{\beta\gamma}$ [see Eq. (A1)] there is only one maximum.³⁹ The position and shape of the peak is determined by two factors: (i) how fast the mass spectrum rises from threshold, $\epsilon_{\beta\gamma}^{(t)} = m_\beta + m_\gamma$, and (ii) how fast the mass spectrum vanishes at the upper limit, $\epsilon_{\beta\gamma}^{(u)} = w - m_\alpha$. Clearly, the faster the mass spectrum rises from threshold and the faster it falls to zero again, then the sharper and closer to threshold is the resultant peak. Furthermore, if the rise from threshold and the falloff at high masses are s -independent, then so is the resultant peak. This, we believe, is the basic kinematic mechanism that controls the Deck effect. Now, we consider, qualitatively, contributions to N , \mathcal{P} , \mathcal{F} , \mathcal{R} for each model.

For model (iv) of Eq. (8), explicit forms are obtained. With no spin and s -wave dissociation, we set $N=1$ and $\mathcal{R} = \text{constant}$;

$$\mathcal{P} = 1/(s_{\beta\gamma} - m_\rho^2)^2$$

and

$$\mathcal{F} = \exp(\eta) \times \{1 - \exp[\bar{a}(t_{\rho\alpha}^{(+)} - t_{\rho\alpha}^{(-)})]\}/\bar{a}, \quad (11)$$

where

$$\eta = -\bar{a}m_\rho^2/(s\mathcal{P}).$$

The form for \mathcal{F} is valid for $m_p = m_\alpha$ and $\epsilon_{\beta\gamma}$ not near the upper limit $\epsilon_{\beta\gamma}^{(u)}$. Models (i), (ii), and (iii) are contained in Eq. (11) as obvious approximations. The only contribution to growth at high $\epsilon_{\beta\gamma}$ comes from the threshold phase space factor $|\vec{\gamma}|$ but \mathcal{O} contains more than sufficient inverse powers of $\epsilon_{\beta\gamma}$ to compensate. This resultant suppression of high $\epsilon_{\beta\gamma}$ states by \mathcal{O} is, furthermore, s -independent. There is an additional damping at high $\epsilon_{\beta\gamma}$ from \mathcal{F} , but this damping can be seen from Eq. (11) to become less effective with increasing s . For this model then, \mathcal{O} is providing the s -independent damping of high $\epsilon_{\beta\gamma}$ and is the controlling mechanism of the Deck effect, as argued by Stodolsky. On the other hand, we see that peaks controlled by \mathcal{F} [see models (i) and (ii) in Fig. 4] are generally farther out, wider, and more importantly, s -dependent.

The spinless version of our model is slightly more complicated. The approximation in Eq. (7) is not used, but no explicit forms like Eq. (11) are obtained. Furthermore, the cutoff k^c in Eq. (4) contributes to \mathcal{F} , though it also becomes less effective as s increases. Nevertheless, our explicit calculation (see Figs. 4 and 8) shows that the mass spectrum is essentially still governed by the Stodolsky mechanism. With \mathcal{O} controlling the high $\epsilon_{\beta\gamma}$ behavior, the resultant peak behaves like a genuine resonance with a slight dependence on s and the parameters of \mathcal{R} and \mathcal{F} .⁴⁰

The single peripheral model Eqs. (2), (5) has a ρ spin which will generally contribute powers of $\epsilon_{\beta\gamma}$ to $d\sigma/d\epsilon_{\beta\gamma}$, leading to growth at high $\epsilon_{\beta\gamma}$. For example, if the $\beta\text{-}\gamma$ system is in p wave [as in diagram 1(A)], then $N=3$ instead of $N=1$. Not only is the rise from threshold slower, but so is the damping at high $\epsilon_{\beta\gamma}$. Spin contributes additionally to \mathcal{R} . The external ρ in each diagram contribute⁴¹ a factor proportional to $\epsilon_{\beta\gamma}^4$. The virtual ρ in diagram 1(C), being elementary, further compounds the difficulty by contributing another factor of $\epsilon_{\beta\gamma}^4$. Just the contribution to \mathcal{R} from the external ρ spin is sufficient to neutralize the propagator factor \mathcal{O} as the dominant high $\epsilon_{\beta\gamma}$ damping mechanism. This is why the Stodolsky mechanism fails to operate in our model with spin. The damping is now controlled by whatever else contributes to \mathcal{R} and \mathcal{F} . Our experience with models (i)–(iv) above suggests that diffraction scattering probably cannot provide an s -independent damping mechanism in \mathcal{F} for the simple kinematical reason that after integration over $t_{p\alpha}$, both $t_{p\alpha}^{(+)}$ and $t_{p\alpha}^{(-)}$ have their s and $\epsilon_{\beta\gamma}$ dependences interwound. Even at fixed s , the resultant peak will be farther out and flatter. We suspect that the same will be true of a form factor that is a function of one momentum-transfer variable only.¹⁹ A more ambitious way would

be to incorporate into \mathcal{F} final-state interaction effects on the mass spectrum. Such a correction can be applied in the form of a DWBA⁴² for example. Being a correction at high $\epsilon_{\beta\gamma}$ values, it will not change the character of our amplitude as a possible background to any genuine diffractively-produced resonance occurring at lower $\epsilon_{\beta\gamma}$ values, but will supply a much sharper suppression of the high $\epsilon_{\beta\gamma}$ states in the background amplitude since it is well-known from 2–2 reactions that DWBA provides a much sharper cutoff⁴² in the relevant momentum-transfer variable than the usual form factor. Unfortunately, we also learn from 2–2 reactions that DWBA-type corrections are not very effective⁴² when high spin exchanges are involved. Thus for our model, a DWBA-type consideration would still be inadequate for diagram 1(C).

It is fitting at this point to add to our comments in the Introduction on Reggeized double peripheral^{7,8} and dual¹³ models. We question there why it should work at low subenergies. But, from the point of view of finding more damping at high subenergies, a Reggeized model would be a good candidate indeed since, being double peripheral, it is presumably valid in this region. By abandoning the elementarity of the virtual particle, a Reggeon model suppresses the contribution to \mathcal{R} due to high spin exchange in the cross channel such as in diagram 1(C) by introducing the Regge factor $(\epsilon_{\beta\gamma})^{i\alpha_\rho(t_{q\gamma})}$, where α_ρ is the ρ trajectory. Even for spinless exchange, the corresponding Regge factor will contribute to \mathcal{F} by suppressing high $\epsilon_{\beta\gamma}$ states through its coupled dependence of the subenergy and momentum-transfer variables. Such suppression is much more effective than that provided by diffractive scattering or the usual form factors. The resultant peak, whether s -dependent or not, is expected to be comparatively sharper and closer to threshold than the one for the corresponding elementary-particle model. We emphasize that, interpreted this way, the use of a Reggeized mechanism is a kinematic explanation of the Deck effect. No dynamic concept such as duality,¹⁰ global or local, need be invoked. In particular, no sequence of peaks is expected as in local duality^{10,13}; and, for a nondiffractive dissociation process involving charge exchange, since duality is not invoked, one is not involved in the question of exotic resonances.¹²

However, the Reggeized Deck effect is still predicated on the assumption that the Regge factor, together with the propagator factor \mathcal{O} not only can cancel any effect of a rising mass spectrum due to spin effects in \mathcal{R} , but has enough inverse powers of $\epsilon_{\beta\gamma}$ left at high $\epsilon_{\beta\gamma}$ to still dominate over other damping effects, such as form factor, diffraction scattering, or phase space, which are generally

s -dependent. This may not be always possible. Unfortunately, in Reggeized calculations done so far,^{3,7,8,13} the spin of the external particle involved in the dissociation (ρ in our case) has usually been ignored. As we have pointed out before, had we ignored external spin in our elementary particle model, we would have obtained s -independent peaks for all diagrams except 1(C) where there is a virtual vector meson. In particular, we see little difference between our model with a form factor and a Reggeized version for diagram 1(B) if the spin of the external particle ρ is not considered. In our model, the external ρ spin contribution in diagram 1(B) completely cancels the damping effect of the propagator at high $\epsilon_{\beta\gamma}$. For the corresponding Reggeized model, an additional, but mild, damping is provided by a π -Regge factor $(\epsilon_{\beta\gamma})^{4\alpha_{\pi}(t_{\alpha\beta})}$ estimated³² to be approximately $(\epsilon_{\beta\gamma})^{-0.6}$. Whether this factor is sufficient to dominate at high $\epsilon_{\beta\gamma}$ the s -dependent damping of diffraction scattering, etc., mentioned above is not clear without numerical calculations. But, regardless of this, what is clear is that, with the inclusion of spin, the resultant weaker damping at least implies a peak much wider and farther out than is claimed in the spinless Reggeized calculations of diagram 1(B). Besides, the usual practice in these calculations to "isolate" particular diagrams as being dominant through cuts in momentum-transfer variables is questionable since it has been demonstrated in explicit calculations⁴³ that all diagrams are comparable in magnitude and similar in the predicted mass spectra. Moreover, as emphasized by Gottfried and Jackson,⁴⁴ the consideration of external spin is particularly important in the case where the external particle is a resonance and its subsequent decay is analyzed to provide information on the production mechanism of the resonance itself. In short, we believe that Reggeon exchange can be an attractive and efficient way to obtain more high $\epsilon_{\beta\gamma}$ damping in order to generate a low $\epsilon_{\beta\gamma}$ peak. But, besides the question of why it can be extended to low $\epsilon_{\beta\gamma}$ values, it has yet to be demonstrated that external spin is indeed a "nonessential complication" that causes no difficulties in such a model. We believe otherwise.

V. CONCLUSION

Our discussions on the momentum-transfer slope and on the question of helicity conservation lead us to conclude that one should be wary of tests based on "expected" properties of the diffraction-dissociation process which are expected only under restrictive kinematic conditions. For example, in our model if Eq. (7) does not hold, then

one cannot expect ϕ isotropy in the Gottfried-Jackson frame, or θ isotropy, or b in Eq. (9) being equal to the input slope. To be sure, such expected properties are intuitively appealing because they are easy to understand and visualize. However, the fact that these "expected" properties are not realized at the energies considered cautions us that physically, the target nucleon is still playing an active role and that diagrams of topology 1(B) cannot yet be reduced, via duality or Eq. (7) to simpler diagrams of topology 1(A). The failure of "expected" properties to occur is also found in the mass spectrum peak. To understand the failure of our model, we have argued that it is not the closeness of the final (π - ρ) state to the initial (π) state which is expected to cause peaking at low masses²⁴ but rather, the damping at high masses. Within the many possible ways to damp high masses is surely hidden a cure for the s dependence. So, the failure of our model at high masses is again a warning that it is unreasonable to expect a single peripheral process to hold outside its kinematic region of established validity—low masses—without significant modifications. Indeed, to stretch the point further, one may well suspect the "expectation" that diagrams like 1(B) or 1(C), however modified at high mass, can and should account for the *entire* mass spectrum, and thus the total production cross section, since at high masses—in the double peripheral region—diagrams like (D) and (E) in Fig. 1 and other competing processes can no longer be neglected.¹⁷ Our point here is that the failure of the single peripheral process to reproduce a peak at low masses is not fatal since the mechanism for the peak eventually involves considerations of competing processes outside its region of claimed validity—low masses in a subsystem. Within this region however, the single peripheral process should still be useful in analyzing angular and momentum-transfer distributions, and especially decay distributions, since spins are easy to account for in this model. In fact, our model, without form factors, has been compared directly with experiments on the dissociations $\pi \rightarrow \pi\rho$ (Ref. 45) and $K \rightarrow K^*\pi$.^{46,47} It is found that a reasonable fit to momentum-transfer, angular, and decay distributions at low masses can be obtained.^{46,47} However, the predicted mass spectrum is found to have a much slower falloff at higher masses^{45,47} and to exhibit an unreasonable dependence on incident energies.⁴⁷ Reggeized models,³ as calculated, exhibit no such s dependence. However, our analyses have demonstrated where this s dependence is coming from—the presence of spin—and that the s independence in Reggeized models is not really established until external spins are accounted for.

ACKNOWLEDGMENT

The author wishes to thank Professor Marc Ross for many enlightening conversations and much encouragement throughout the course of this work. The helpful assistance of the staff at the William and Mary Computing Center is gratefully acknowledged.

APPENDIX

The process (i) is written:

$$\pi(q) + N(p) \rightarrow N(\alpha) + \rho(\beta) + \pi(\gamma),$$

where $(p, q, \alpha, \beta, \gamma)$ are each a collective label for the four-momenta, spin, and internal quantum numbers of the respective particles. We employ a metric such that $\alpha^2 = \vec{\alpha}^2 - \alpha_0^2 = -m_\alpha^2$, m_α being the mass of particle α . The virtual particles in diagrams (A), (B), (C) of Fig. 1 are, for our model, π, π, ρ and their masses are denoted m_A, m_B, m_C , respectively. We use values where m (proton) = 938.2 MeV, $m(\rho)$ = 760 MeV, and $m(\pi)$ = 139.6 MeV. Kinematic invariants of interest are $s = -(p+q)^2$, $s_{\alpha\beta} = -(\alpha+\beta)^2$, etc., $t_{q\alpha} = -(q-\alpha)^2$, etc., and $t_{p\alpha} = -(p-\alpha)^2$, etc. The polarization vectors of the ρ meson are denoted ϵ^λ . We shall have occasion to evaluate quantities in the laboratory ($\vec{p}=0$) frame and the over-all center-of-mass ($\vec{p}+\vec{q}=0$) frame. In such cases, we use an explicit subscript, viz. $(\alpha_0)_{\vec{p}+\vec{q}=0}$ is the energy of particle α in the $\vec{p}+\vec{q}=0$ frame. Otherwise, quantities without such subscripts are to be evaluated in the π - ρ rest ($\vec{\beta}+\vec{\gamma}=0$) frame. The orientation of the $\vec{\beta}+\vec{\gamma}=0$ frame is chosen to coincide with a Gottfried-Jackson frame³⁵ illustrated in Fig. 2.

The input variables to Eq. (1) are $|\vec{q}|_{\vec{p}=0}$ (the incident momentum), $\epsilon_{\beta\gamma}$ (the β - γ invariant mass), $t_{p\alpha}$ (square of the four-momentum transfer from p to α), and $\theta_\gamma, \phi_\gamma$ (the angles in the β - γ rest frame). Their ranges are:

$$\begin{aligned} 0 &\leq |\vec{q}|_{\vec{p}=0} \leq \infty, \\ \epsilon_{\beta\gamma}^{(t)} &\leq \epsilon_{\beta\gamma} \leq \epsilon_{\beta\gamma}^{(u)}, \\ t_{p\alpha}^{(-)} &\leq t_{p\alpha} \leq t_{p\alpha}^{(+)}, \\ 0 &\leq \theta_\gamma \leq \pi, \\ 0 &\leq \phi_\gamma \leq 2\pi, \end{aligned} \quad (\text{A1})$$

where:

$$\begin{aligned} \epsilon_{\beta\gamma}^{(u)} &= w - m_\alpha, \\ \epsilon_{\beta\gamma}^{(t)} &= m_\beta + m_\gamma, \\ t_{p\alpha}^{(\pm)} &= (m_p^2 + m_\alpha^2 - 2p_0\alpha_0 \pm 2|\vec{p}| |\vec{\alpha}|)_{\vec{p}+\vec{q}=0}, \end{aligned} \quad (\text{A2})$$

and

$$\begin{aligned} w^2 &= m_p^2 + m_q^2 + 2m_p(q_0)_{\vec{p}=0}, \\ (p_0)_{\vec{p}+\vec{q}=0} &= (s + m_p^2 - m_q^2)/2w, \\ (\alpha_0)_{\vec{p}+\vec{q}=0} &= (s + m_\alpha^2 - s_{\beta\gamma})/2w, \\ s_{\beta\gamma} &= \epsilon_{\beta\gamma}^2, \\ s &= w^2. \end{aligned} \quad (\text{A3})$$

Given a set of values for the input variables, we can specify a momentum configuration for $q+p \rightarrow \alpha+\beta+\gamma$ in the $\vec{\beta}+\vec{\gamma}=0$ frame (see Fig. 2). Let any three-vector \vec{v} be written as $\vec{v} = (v_x, v_y, v_z)$, then:

$$\begin{aligned} \vec{q} &= |\vec{q}| (0, 0, 1), \\ \vec{\alpha} &= |\vec{\alpha}| (\sin\theta_{\alpha q}, 0, \cos\theta_{\alpha q}), \\ \vec{\gamma} &= |\vec{\gamma}| (\sin\theta_\gamma \cos\phi_\gamma, \sin\theta_\gamma \sin\phi_\gamma, \cos\theta_\gamma), \\ \vec{\beta} &= -\vec{\gamma}, \\ \vec{p} &= \vec{\alpha} + \vec{q}, \end{aligned} \quad (\text{A4})$$

where:

$$\begin{aligned} \alpha_0 &= (s - m_\alpha^2 - s_{\beta\gamma})/2\epsilon_{\beta\gamma}, \\ \beta_0 &= (s_{\beta\gamma} + m_\beta^2 - m_\gamma^2)/2\epsilon_{\beta\gamma}, \\ \gamma_0 &= \epsilon_{\beta\gamma} - \beta_0, \\ q_0 &= (s_{\beta\gamma} + m_q^2 - t_{p\alpha})/2\epsilon_{\beta\gamma}, \\ p_0 &= (s_{\beta\gamma} + m_p^2 - t_{p\alpha})/2\epsilon_{\beta\gamma}, \\ \cos\theta_{\alpha q} &= (t_{q\alpha} - m_\alpha^2 - m_q^2 - 2\alpha_0 q_0)/(2|\vec{\alpha}| |\vec{q}|). \end{aligned} \quad (\text{A5})$$

Note that the momentum-transfer variables $t_{q\beta}$ and $t_{q\gamma}$ are dependent on the polar angle θ_γ , but the subenergy variables $s_{\alpha\beta}$ and $s_{\alpha\gamma}$ are additionally dependent on the azimuthal angle ϕ_γ .

*Work supported in part by the National Science Foundation.

¹M. L. Good and W. D. Walker, Phys. Rev. **120**, 1857 (1960).

²D. R. O. Morrison, Phys. Lett. **22**, 528 (1966).

³For an extensive summary of experiments as well as recent theoretical calculations on the A_1, Q , and $N^*(1470)$ enhancements, see Particle Data Group, Phys. Lett. **39B**, 1 (1972).

⁴R. T. Deck, Phys. Rev. Lett. **13**, 169 (1964). See also

- U. Maor, Ann. Phys. (N.Y.) 41, 456 (1967).
- ⁵M. Ross and Y. Y. Yam, Phys. Rev. Lett. 19, 546 (1967). We refer to this paper as RY. Earlier references to the Deck effect are given here.
- ⁶See for example, J. Gillespie, *Final State Interactions* (Holden-Day, San Francisco, 1964); see also M. M. Islam [Phys. Rev. 131, 2292 (1963)] and J. G. Rushbrooke [Phys. Rev. 177, 2357 (1969)] for applications to the $N \rightarrow N^*(1470)$ process.
- ⁷For a prototype calculation in which the virtual π [diagram 1(B)] is Reggeized, see E. L. Berger, Phys. Rev. 166, 1525 (1968). For applications of the Reggeized π to other reactions see Ref. 3.
- ⁸For a prototype calculation in which both the virtual π [diagram 1(B)] and ρ [diagram 1(C)] are Reggeized, see G. W. Brandenburg *et al.*, Nucl. Phys. B16, 369 (1970). For other processes, see Ref. 3.
- ⁹G. Chew and A. Pignotti, Phys. Rev. Lett. 20, 1078 (1968).
- ¹⁰R. Dolen, D. Horn and C. Schmid, Phys. Rev. 166, 1768 (1968); G. Veneziano, Nuovo Cimento 57A, 190 (1968). The different concepts of duality in these two papers are often referred to as global duality and local duality, respectively.
- ¹¹See for example, J. Pumplin, Phys. Rev. D 7, 795 (1973).
- ¹²D. Cohen *et al.*, Phys. Rev. Lett. 28, 1601 (1972).
- ¹³($pp \rightarrow pn\pi^+$): S. Pokorski and H. Satz, Nucl. Phys. B19, 113 (1970); ($K^-p \rightarrow pK^-\pi^+\pi^-$): Aachen-Berlin-CERN-London-Vienna collaboration, *ibid.* B24, 221 (1970); ($\gamma p \rightarrow \pi^+\pi^-p$): G. Kramer and H. R. Quinn, *ibid.* B27, 77 (1971).
- ¹⁴G. Wolf, Phys. Rev. 183, 1538 (1969).
- ¹⁵B.-L. Young, J. T. Donohue, and R. F. Peierls, Phys. Rev. D 3, 2801 (1971).
- ¹⁶F. Gilman, J. Pumplin, A. Schwimmer, and L. Stodolsky, Phys. Lett. 31B, 387 (1970).
- ¹⁷See, G. Cohen-Tannoudji, G. Kane, and C. Quigg [Nucl. Phys. B37, 77 (1972)] for arguments that non-diffractive exchanges may be important.
- ¹⁸ F_B is taken from H. P. Dürr and H. Pilkuhn, Nuovo Cimento 40A, 899 (1965).
- ¹⁹See, e.g., J. C. Vander Velde *et al.* [Univ. of Michigan report 1971 (unpublished)], where a Reggeized form factor is used for the process $n \rightarrow p\pi$ in scattering off heavy nuclei.
- ²⁰J. D. Jackson and H. Pilkuhn, Nuovo Cimento 33, 906 (1964).
- ²¹J. Benecke and H. P. Dürr, Nuovo Cimento 56A, 269 (1969).
- ²²In many theoretical calculations using the Monte Carlo method, it is often necessary to impose cuts on some momentum-transfer variables, in direct simulation of experimental procedures. Such cuts in a theoretical calculation should be considered as being equivalent to form factors with step-function cutoffs. We do not use a Monte Carlo method in our calculation.
- ²³The value for $g_{\rho\pi\pi}$ is fixed by the ρ width. For data on π , see K. J. Foley *et al.*, Phys. Rev. Lett. 11, 425 (1963). For data on ρ , see Aachen-Berlin-Bonn-Hamburg-Heidelberg-München collaboration, Phys. Rev. 175, 1669 (1968).
- ²⁴L. Stodolsky, Phys. Rev. Lett. 18, 973 (1967).
- ²⁵See for example, A. H. Rosenfeld in *Proceedings of the Oxford International Conference on Elementary Particles*, 1965, edited by T. Walsh *et al.* (Rutherford High Energy Laboratory, Chilton, Didcot, Berkshire, England, 1966).
- ²⁶B. Y. Oh and W. D. Walker, Phys. Lett. 28B, 564 (1969).
- ²⁷I. M. Blair *et al.*, Phys. Rev. Lett. 17, 789 (1966); K. J. Foley *et al.*, Phys. Rev. Lett. 19, 397 (1967).
- ²⁸See Ref. 3, and Aachen-Berlin-CERN collaboration, Nucl. Phys. B8, 45 (1968).
- ²⁹M. Elitzur, Phys. Rev. Lett. 27, 895 (1971).
- ³⁰The $N^*(1470)$ is excluded by Elitzur (Ref. 29) because its slope is experimentally (see Ref. 27) larger. This is another indication that this enhancement should be associated with a diffraction-dissociation process which predicts slopes generally larger than the input value.
- ³¹This subjected, as usual, to modifications by spin and form-factor effects. Note, for example, that diagram 1(C), with a virtual ρ , has a slope less than the input value (see Fig. 5).
- ³²E. L. Berger, Phys. Rev. 179, 1567 (1969).
- ³³R. E. Waltz, Phys. Lett. 30B, 490 (1969); S. Pokorski, M. Szeptycka, and A. Zieminski, Nuovo Cimento 69A, 290 (1970).
- ³⁴The numerical value for the slope is expected to be much larger for nuclear targets [see, e.g., Orsay-Milan-Saclay-Berkeley collaboration, Nuovo Cimento 46A, 737 (1966)], since the input nuclear diffraction slope is also much larger.
- ³⁵K. Gottfried and J. D. Jackson, Nuovo Cimento 33, 309 (1964).
- ³⁶Aachen-Berlin-Bonn-CERN-Cracow-Heidelberg-London-Vienna collaboration, Phys. Lett. 34B, 160 (1971).
- ³⁷Incidentally, if we consider the ϕ distribution in the α - γ rest frame for diagram 1(B), then we obtain a test of the virtual pion spin. For our elementary particle model, a flat ϕ distribution is expected, but for a Reggeon model (see Ref. 32) anisotropy is expected. However, in comparing with experimental data, one must additionally consider diagrams 1(A) and 1(C) in our model (see Ref. 43). ϕ isotropy is lost if the virtual particle has spin.
- ³⁸As an indication of the ambiguity, we note that by using a Wolf background (Ref. 14), J. Ballam *et al.*, [Phys. Rev. Lett. 21, 934 (1968)] favor a 1^+ (d -wave) assignment for the A_1 as a genuine resonance. On the other hand, G. W. Brandenburg *et al.* [Nucl. Phys. B16, 287 (1970)] found that their data favor a 1^+ (s -wave) assignment with no separation into background and resonance. See, also, C. D. Froggatt and G. Ranft [Phys. Rev. Lett. 23, 943 (1969)], who found a 1^+ (s -wave) assignment and a semilocal duality (see Ref. 9) interpretation with a Reggeized amplitude.
- ³⁹Local dual models do not satisfy the smoothness condition and have many peaks.
- ⁴⁰As s approaches infinity, the peak will move out and broaden slightly, but will approach the finite limits established without the additional s -dependent damping.
- ⁴¹The external ρ will contribute a spin factor proportional to $\epsilon_{\beta\gamma}^4$, except when the momentum transfer to the ρ is kept at its minimum value.
- ⁴²For an extensive list of references on the distorted-wave Born approximation (DWBA) in high-energy physics, see J. D. Jackson in Rev. Mod. Phys. 37, 484 (1965).
- ⁴³N. M. Carson *et al.*, Phys. Rev. Lett. 18, 880 (1967);

G. Fraser and R. Roberts, *Nuovo Cimento* **47A**, 293 (1967); G. W. Brandenburg *et al.*, Ref. 8; J. A. Gaido *et al.*, *Nucl. Phys.* **B23**, 84 (1970). See also Sec. III in this paper.

⁴⁴K. Gottfried and J. D. Jackson, *Nuovo Cimento* **34**,

735 (1964).

⁴⁵See G. W. Brandenburg *et al.*, Ref. 8.

⁴⁶J. C. Park *et al.*, *Phys. Rev. Lett.* **20**, 171 (1968).

⁴⁷F. Bomse *et al.*, *Phys. Rev. Lett.* **20**, 1519 (1968).

PHYSICAL REVIEW D

VOLUME 8, NUMBER 5

1 SEPTEMBER 1973

$\rho\pi\pi$ Regge Residue Function from a New Class of Sum Rules, and a New Representation for $\pi\pi$ Amplitudes

E. P. Tryon

Department of Physics and Astronomy,

Hunter College of the City University of New York, New York, New York 10021

(Received 29 June 1972; revised manuscript received 19 April 1973)

A new class of sum rules is developed within the context of the $\pi\pi$ system. One of these sum rules is used to extract the $\rho\pi\pi$ Regge residue function from the recent $\pi\pi$ data of Carroll *et al.*, for a wide range of momentum transfer. The residue has a zero near $t = -0.5$ GeV^2 , in agreement with duality and with a new prediction which we make from the dual absorption model together with πp and $\bar{p}p$ data. The $\pi\pi$ charge-exchange amplitude is shown to be dominated by ρ exchange above 1.0 GeV. We also derive a new representation which expresses $\pi\pi$ amplitudes in terms of a single subtraction parameter and integrals over physical-region absorptive parts. The representation is valid over a substantial portion of the physical region, and constitutes a powerful tool for studying the $\pi\pi$ interaction. Finally, we show that a unitarized Veneziano model proposed earlier by the present author is an excellent approximation to nature below about 800 MeV, despite its neglect of Pomeranchon exchange and $K\bar{K}$ production.

I. INTRODUCTION AND SUMMARY

Standard assumptions of S-matrix theory enable us to express scattering amplitudes in terms of fixed- s dispersion relations (D.R.'s) and alternatively, in terms of fixed- t D.R.'s. By taking differences between such D.R.'s, it is possible to eliminate the subtraction terms, and thereby obtain sum rules equating certain integrals over absorptive parts to zero.

In the present paper, we apply this technique to the $\pi\pi$ system. We obtain sum rules which are similar to, but more powerful than, the sum rules of Wanders,¹ Roskies,² and Roy.³ We use one of these sum rules to extract the $\rho\pi\pi$ Regge residue function from the recent $\pi\pi$ data of Carroll *et al.*,⁴ and obtain results with uncertainties of the order of 10%. The residue has a zero near $t = -0.5$ GeV^2 , in agreement with duality and with a new prediction which we make from the dual absorption model⁵ together with πp and $\bar{p}p$ data.

We show that in the sense of local averages, the $\pi\pi$ charge-exchange amplitude of Carroll *et al.* can be well approximated above 1.0 GeV by Reggeized ρ exchange, with our value for the residue function.

We derive a new representation which expresses

$\pi\pi$ amplitudes in terms of a single subtraction parameter and integrals over physical-region absorptive parts. Our representation is valid over the same portion of the physical region as the twice-subtracted representations of Roskies² and Roy,³ and therefore constitutes a powerful tool for studying the $\pi\pi$ interaction.

Finally, we show that a unitarized Veneziano $\pi\pi$ model proposed earlier⁶ by the present author is an excellent approximation to nature below about 800 MeV, despite its neglect of Pomeranchon exchange and $K\bar{K}$ production.

II. DISPERSION RELATIONS AND SUM RULES

We denote the $\pi\pi$ elastic amplitude with isospin I in the s channel by $A^I(s, t)$, and the amplitude with isospin I in the t channel by $T^I(s, t)$. According to standard assumptions⁷ of analyticity and crossing symmetry, the A^I and T^I are related by

$$A^I(s, t) = T^I(t, s), \quad (1a)$$

and also by

$$A^I(s, t) = \sum_{I'=0}^2 C_{II'} T^{I'}(s, t), \quad (1b)$$

where $C = C^{-1}$ denotes the s - t crossing matrix